Effect of interdot coupling on spin-wave modes in nanoparticle arrays

L. Giovannini, F. Montoncello, and F. Nizzoli
Dipartimento di Fisica, Università di Ferrara, Via Saragat 1, I-44100 Ferrara, Italy
(Received 14 August 2006; revised manuscript received 18 October 2006; published 12 January 2007)

We have developed a theory for the determination of the collective spin-wave modes of regular arrays of magnetic particles, taking into account the dipolar interaction among particles. The frequencies and profiles of the spin modes of arrays of permalloy cylindrical particles with different interparticle separation have been calculated with a numerical implementation of this model, using a three-dimensional representation of the magnetic particles in their actual nonuniform fundamental state. The results show a very good agreement with recently published experimental data, and allow us to discuss the dispersion curves and some relevant properties of the Brillouin light-scattering intensity from spin modes in periodic arrays.

DOI: 10.1103/PhysRevB.75.024416 PACS number(s): 75.75.+a, 75.30.Ds, 75.40.Gb, 75.40.Mg

I. INTRODUCTION

In modern miniaturized systems the continuous reduction in the size of electronic and magnetic devices results in increased packing of their constituting elements. In the case of small magnetic elements, possibly used for high-density nonvolatile memories, the vicinity of the particles gives rise to interdot magnetic coupling, that must be understood in order to be able to control its effects. The coupling, mainly of dipolar nature, affects both the static and dynamic behavior of the magnetization. While the static properties of coupled nanoparticles have been often theoretically investigated both analytically[1,2] and by micromagnetic calculations,[3–6] the dynamic behavior is seldom considered. However, the picosecond magnetization dynamics of small magnetic elements supports the operation of future devices and experimental evidence of dynamic coupling has already been obtained, in the form of fourfold anisotropy of square arrays of otherwise circularly symmetric dots.[7–10] A theory of collective spin-wave modes of arrays made of spherical particles has been recently developed;[11,12] the high symmetry of these, also assumed uniformly magnetized, allowed the use of an analytical approach. A drawback of these assumptions is the limited range of applicability of this theory; in particular, the experimental data presently available refer to particles with planar structure and nonuniform magnetization. A numerical approach to the calculation of collective modes of an array, based on a time-domain micromagnetic simulation followed by Fourier transform, was applied to a system made of a finite number of particles (nine).[13] Despite the relevant calculation effort due to the lack of translational invariance, the number of particles considered in that simulations was too small to efficiently mimic the real system. The comparison with experimental data allowed the authors to reproduce the general behavior of the mode frequencies as a function of the interdot separation, but the mode assignment was questionable and the fine structure of the bands was missing or incomplete. The case of coupled disks in the vortex state have been investigated studying the lowest frequency (so-called gyrotropic) mode[14] and also higher modes;[15] in both cases the applied field is zero and the same fundamental state is assumed for all the dots in the array. The collective behavior of an array of single domain magnetic particles with uniform static and dynamic magnetization has been studied by Politi and Pini[16] with no applied field.

In this paper we present a theoretical model for calculating the collective modes of infinite arrays of arbitrary shaped particles with an applied field, based on the numerical solution of the magnetic dynamical matrix[17] of the system. The actual static magnetization of the particles is fully taken into account, by assuming that it is the same for all the particles in the array; the dynamic magnetization is written in the Bloch form, so that the total number of independent variables is limited also for infinite arrays and the numerical calculation remains feasible. An application is presented to a square array of cylindrical particles, a system whose collective spin mode frequencies measured by Brillouin light scattering (BLS) are available.[13] The comparison between the theoretical results and the experimental data confirms the validity of the model.

II. THEORY

The spin normal modes of a single magnetic nanoparticle of arbitrary shape can be calculated by using a dynamical matrix method.[17–19] Within this approach, the particle is divided into N cells within which the magnetization is assumed constant; therefore the $2N$ variables of the problem are the two polar angles ϕ_j and θ_j of the magnetization in each cell j. The Zeeman, exchange, and demagnetizing interactions within the particle are taken into account, and a linearized dynamical matrix whose eigenvalues and eigenvectors correspond to the spin-mode frequencies and profiles, respectively, can be set up. In this section we extend this model by including the dipolar interdot coupling.

We assume that the nanoparticles form a bidimensional infinite array with primitive vectors $\boldsymbol{a}_1$ and $\boldsymbol{a}_2$, and base vectors of the reciprocal lattice $\boldsymbol{b}_1$ and $\boldsymbol{b}_2$. As a first step, the static magnetization is calculated for a single dot using a standard micromagnetic technique with periodic boundary conditions, with the same periodicity of the array. Therefore we assume that the fundamental state is the same for all particles. This condition must be carefully considered; it is well known, for example, that an array of free planar magnetic dipoles takes ferromagnetic or antiferromagnetic configurations according to the lattice symmetry (triangular or

square lattice),[16,20,21] with some additional effects due to the boundary conditions in finite lattices.[22,23] In addition, other effects must be taken into account. For example thin circular dots are known to undergo several transitions as the external field increases.[24] At zero field, a vortex structure can be found in each particle; if the interparticle interaction is negligible, both vortex core polarization and chirality are oriented at random, whereas the interdot coupling induces some correlation. However, for close and small enough circular dots, finite-size effects plays an important role; for example a sort of supervortex of the whole array may form, where each dot has a quasiuniform magnetization.[23] Also other superdomain configurations are possible, with domains extended to the whole array. When a field is gradually applied, the static magnetization of each dot changes, until the whole system reach saturation. The last situation assures an identical magnetization of all particles, as required by our model. The occurrence of this condition can be verified, from a theoretical point of view, by comparing the dipolar interdot coupling field with the external field[25] or by finding a purely real spin-wave frequency,[16] and, from an experimental point of view, by either checking the magnetic configuration of the array by maagnetic force microcoscopy (MFM) or by evaluating by Kerr effect the field required to obtain the full saturation of the sample.

The fluctuation of the magnetization with respect to the fundamental state can then be written in the Bloch form:

$$\delta \boldsymbol{m}(\boldsymbol{r}+\boldsymbol{R}) = e^{i\boldsymbol{K}\cdot\boldsymbol{R}}\delta\boldsymbol{m}(\boldsymbol{r}), \tag{1}$$

where $\boldsymbol{R}$ is a lattice vector and $\boldsymbol{K}=(K_x,K_y)$ is a Bloch vector (taken in the first Brillouin zone of the array) which, according to the standard periodic boundary conditions, is given by

$$\boldsymbol{K} = \frac{n_1}{M_1}\boldsymbol{b}_1 + \frac{n_2}{M_2}\boldsymbol{b}_2, \quad n_i \in \mathbb{Z}, \quad n_i = -\frac{M_i}{2}, \ldots, \frac{M_i}{2} - 1;$$

here M_1 and M_2 represent the actual numbers of particles of the array in the direction of $\boldsymbol{a}_1$ and $\boldsymbol{a}_2$, respectively. In Eq. (1) $\boldsymbol{r}$ can be restricted to a single particle, so that its magnetization determines that of the whole system (for any given Bloch wave vector). This means, as for the case of independent particles, that also in the periodic array there are $2N$ independent variables, corresponding to the orientation of the magnetization of the N cells of just one particle. Now we can write the motion equations of the magnetization of the system, where the independent variables are the small deviations from equilibrium $\delta\phi_j$ and $\delta\theta_j$ for every cell j of the particle at $\boldsymbol{R}=0$:

$$\begin{aligned}
&\sum_{j=1}^{N}\left(-\frac{\sum_{\boldsymbol{R}} E_{\theta_k\phi_{j\boldsymbol{R}}}e^{i\boldsymbol{K}\cdot\boldsymbol{R}}}{\sin\theta_k}\right)\delta\phi_j + \sum_{j=1}^{N}\left(-\frac{\sum_{\boldsymbol{R}} E_{\theta_k\theta_{j\boldsymbol{R}}}e^{i\boldsymbol{K}\cdot\boldsymbol{R}}}{\sin\theta_k}\right)\delta\theta_j \\
&\quad - \lambda\,\delta\phi_k = 0, \quad k = 1,\ldots,N, \\
&\sum_{j=1}^{N}\frac{\sum_{\boldsymbol{R}} E_{\phi_k\phi_{j\boldsymbol{R}}}e^{i\boldsymbol{K}\cdot\boldsymbol{R}}}{\sin\theta_k}\delta\phi_j + \sum_{j=1}^{N}\frac{\sum_{\boldsymbol{R}} E_{\phi_k\theta_{j\boldsymbol{R}}}e^{i\boldsymbol{K}\cdot\boldsymbol{R}}}{\sin\theta_k}\delta\theta_j - \lambda\,\delta\theta_k = 0, \\
&\quad k = 1,\ldots,N.
\end{aligned} \tag{2}$$

Here $\lambda = iM_s\Omega/\gamma$, M_s is the saturation magnetization, Ω is the frequency, γ is the gyromagnetic ratio, and the sums run over all $\boldsymbol{R}$ in the array. The quantities $E_{\alpha_k\beta_{j\boldsymbol{R}}}$ are the second derivatives of the energy, with respect to the angle α_k of the particle in $\boldsymbol{R}=0$ and the angle β_j of the particle in $\boldsymbol{R}$. Equations (2) should be compared with Eqs. (3) of Ref. 17, concerning a single independent particle. The total energy of the system (divided by the cell volume) E includes Zeeman, exchange, and dipolar energies. We assume that the magnetic particles do not touch, so that there is no interdot exchange coupling. Therefore the Zeeman and the nearest-neighbor exchange energy derivatives (see Appendix B of Ref. 17) do not contribute to the terms with $\boldsymbol{R}\neq 0$ in Eq. (2) and the expressions of the derivatives given in Ref. 17 are still usable. The dipolar energy of the system now is

$$E_{\mathrm{dip}} = \frac{M_s^2}{2}\sum_{k,j=1}^{N}\sum_{\boldsymbol{R},\boldsymbol{R}'}\boldsymbol{m}_k(\boldsymbol{R})\overleftrightarrow{N}(\boldsymbol{R},\boldsymbol{R}',k,j)\boldsymbol{m}_j(\boldsymbol{R}'),$$

where $\overleftrightarrow{N}(\boldsymbol{R},\boldsymbol{R}',k,j)$ is the demagnetizing tensor,[26,27] coupling the cell k of the particle in $\boldsymbol{R}$ with the cell j of the particle in $\boldsymbol{R}'$. Using Eq. (1) and exploiting the symmetries of the demagnetizing tensor, the required dipolar second derivatives turn out to be

$$E_{\mathrm{dip}\alpha_k\beta_{j\boldsymbol{R}}} = \begin{cases} M_s^2\left(\sum_{k'=1}^{N}\sum_{\boldsymbol{R}'}\boldsymbol{m}_{k'}\cdot\overleftrightarrow{N}(\boldsymbol{R}',\boldsymbol{0},k',k)\dfrac{\partial^2\boldsymbol{m}_k}{\partial\alpha_k\partial\beta_k} + \dfrac{\partial\boldsymbol{m}_k}{\partial\beta_k}\cdot\overleftrightarrow{N}(\boldsymbol{0},\boldsymbol{0},k,k)\dfrac{\partial\boldsymbol{m}_k}{\partial\alpha_k}\right) & \boldsymbol{R}=\boldsymbol{0} \text{ and } j=k \\ M_s^2\dfrac{\partial\boldsymbol{m}_j}{\partial\beta_j}\cdot\overleftrightarrow{N}(\boldsymbol{R},\boldsymbol{0},j,k)\dfrac{\partial\boldsymbol{m}_k}{\partial\alpha_k} & \text{otherwise.} \end{cases}$$

α and β can be ϕ or θ, the unitary magnetizations appearing here refer to $\boldsymbol{R}=0$, and their partial derivatives are easily obtained from Eq. (2) of Ref. 17 and calculated at equilibrium.

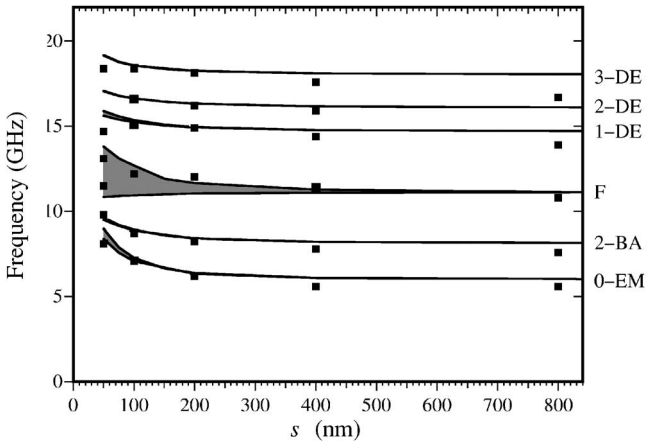

FIG. 1. Frequency dependence of the lowest spin modes on the interdot separation s (lines). At small s the modes form bands, represented by gray areas in the figure. Dots are experimental data, taken from Ref. 13.

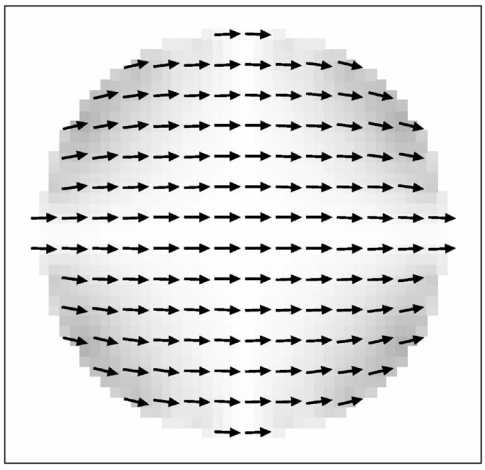

FIG. 2. Static magnetization calculated for an insulated permalloy dot in a 2-kOe applied field (central layer). The geometric and magnetic parameters are given in the text. For the sake of clearness the magnetization of each block of nine cells has been averaged and represented by a single arrow. The static magnetization used in the dynamical simulations depends on the interdot separation, but the dependence is too weak to be perceivable in a graph.

Finally, the analytic expressions of the coefficients of the linear system (2) can be evaluated numerically for a given ground state. As is customary in numerical approaches, the infinite dipolar sums over $\boldsymbol{R}$ and $\boldsymbol{R}'$, which appear in the system and the energy derivatives, are calculated by truncation; in particular we start from the interaction of a cell with its nearest neighbors, then we sum terms corresponding to farther and farther cells; when the contributions become negligible with respect to the machine accuracy, the sums are terminated. It turns out that, typically, particles within $R \leqslant 3a$, with $a_1=a_2=:a$ contribute to the sums. This is also consistent with experimental results showing that elements separated by a distance greater than the dot size do not significantly interact.[28] Note that, although the number of particles needed to achieve convergence is rather small, the number of cells (typically of size 5 nm) is very large, of the order of 10^5, as required by the long-range nature of the dipolar interaction. The system is then reduced to an eigenvalue problem[17] that can be solved numerically, allowing us to obtain the spin-mode frequencies and profiles.

III. RESULTS AND DISCUSSION

The frequencies of the modes of a squared array of permalloy discs are shown in Fig. 1 for different interdot separation. The particles have a cylindrical shape, with thickness 50 nm and radius 100 nm. The x and y axes of the reference frame are parallel to $\boldsymbol{a}_1$ and $\boldsymbol{a}_2$, respectively, while z is perpendicular to the sample; an external field $H=2000$ Oe is applied along the x direction. This field is strong enough to assure the identical static magnetization of all the dots of the array, as experimentally verified[13] and easily understood by comparing the interdot dipolar field, of the order of 100 Oe, with the external field intensity. The calculated static magnetization is shown in Fig. 2. The calculation of the theoretical frequencies has been performed with the model presented in Sec. II, using the following standard values of the magnetic constants of permalloy: $M_s=860$ G, $\gamma=1.838\times10^7$ rad/(s Oe), exchange constant $A=1.3\times10^{-6}$ erg/cm. The particles are placed at the nodes of a square array with $a_1=a_2=a=s+200$ nm, where s is the interdot separation. Due to the relatively large thickness of the discs, a bidimensional model (with cell height equal to the particle height) would be inadequate; therefore we used a three-dimensional (3D) model with three layers of cells in each dot. Despite the modes show some variation of the magnetization profile in the direction perpendicular to the surface, the classification introduced for thin particles[18] is still applicable; however, the 3D approach is essential for a correct reproduction of the experimental frequencies. A detailed study of the dependence of the profile of spin modes on the particle thickness will be presented elsewhere. The cell size is $5\times5\times16.7$ nm^3; we have found that a reduction of the cell height to 10 nm (i.e., by using five layers of cells instead of three) did not give rise to a significant change of the calculated frequencies. The total number of active cells is therefore $N=3792$, for a computation time of about 90 min per run for a PC. In Fig. 1 the frequencies measured by BLS (Ref. 13) in arrays of permalloy particles with the same size as in the calculations are also plotted (dots). The comparison of the measurements with the calculated results allows us to assign the modes. Starting from the lowest frequency, we recognize a laterally localized mode, or end mode of zero order, (0-EM), a backwardlike mode with oscillations along the direction of the applied field (2-BA), the fundamental or quasiuniform mode F and three Damon-Eshbach like modes with oscillations perpendicular to the applied field (1-DE, 2-DE, and 3-DE). The labels are consistent with those introduced for the modes of independent dots[18] and are based on the node-number counting. The BA and DE nomenclature has been adopted for historical reasons from the film waves,[29] although in the case of dots we deal with standing waves, rather than with traveling waves.

For large interdot separation, each mode is characterized by a single frequency: in this limit the coupling is negligible,

and the eigenfrequencies do not depend on $\boldsymbol{K}$. When s becomes comparable to the dot diameter, the interdot coupling gives rise to the appearance of bands; within each band the frequency of the collective modes depends on $\boldsymbol{K}$. The agreement between the calculated curves and the experimental data is very good. There is a general increase of the mode frequencies when s becomes smaller; more precisely, both band center and width change with s, with a trend which varies from one mode to another. The F mode feels the strongest interdot coupling, followed by the 0-EM mode; when the separation equals the dot diameter, the relative band width of the mode F is 5%, that of the 0-EM mode is 0.7%, while for other modes it is $<0.2\%$. The corresponding broadening of the experimental peaks is also visible in the experimental data for $s=50$ nm, as in Fig. 2 of Ref. 13, where the F band extends to the range 11–14 GHz, with a structure given by a few peaks. The strongest coupling of the F and 0-EM mode can be traced to their nonvanishing average magnetization:[18] in this case the coupling between adjacent dots is relatively large, thanks to the dipolar field as demonstrated analytically for a different system by Galkin *et al.*[15] The interdot coupling for the other modes, all having a vanishing or small average magnetization, is weaker and mainly due to the nonuniformity of the dynamic magnetization.

A comparison of our results with those obtained by Gubbiotti *et al.*[13] on a finite (nine dots) bidimensional system with a micromagnetic approach shows that the band opening or width of the F mode in that calculation starts at 200 nm, while in our case is already appreciable at $s=400$ nm; in addition, Fig. 3 of Ref. 13 shows three curves (instead of a band) with a width of about 3.5 GHz at $s=50$ nm instead of 3.0 GHz in our case. However, it should be noted that the simplified micromagnetic approach reproduces the general increase of the mode frequencies as s becomes smaller, although the agreement with experimental results is significantly worse. We have also corrected the assignment of the higher frequency modes, since the BLS cross section of the mixed modes 4-BA×2-DE, 2-BA×2-DE, and of the 4-DE mode mentioned in Ref. 13 is very small and in any case smaller than that of the 1-DE and 3-DE modes. A discussion of the BLS cross section is postponed to the end of this section.

The profiles of the F modes calculated at $s=50$ nm are shown in Fig. 3. The mode calculated for $\boldsymbol{K}=(0,0)$ [Fig. 3(c)] has a positive-definite profile (gray-black), i.e., the dynamic magnetization oscillates in-phase in the whole dot. A comparison with the mode calculated for $\boldsymbol{K}=(0,\pi/a)$ [Fig. 3(a)] evidences that the last possess pronounced oscillations along the y (vertical) direction, with even regions of negative dynamic magnetization (white). As expected, comparable oscillations along x and y are shown by the mode with $\boldsymbol{K}=(\pi/a,\pi/a)$ [Fig. 3(d)]. These oscillations are induced by the coupling with the nearest-neighbor dots oscillating out of phase. The evolution of the F modes with $\boldsymbol{K}=(0,0)$ and $\boldsymbol{K}=(\pi/a,\pi/a)$ is plotted in Fig. 4 as a function of the interdot separation s. Starting from the first row, that corresponds to the modes of an isolated dot, then independent of $\boldsymbol{K}$, the difference between the two columns becomes stronger as s decreases.

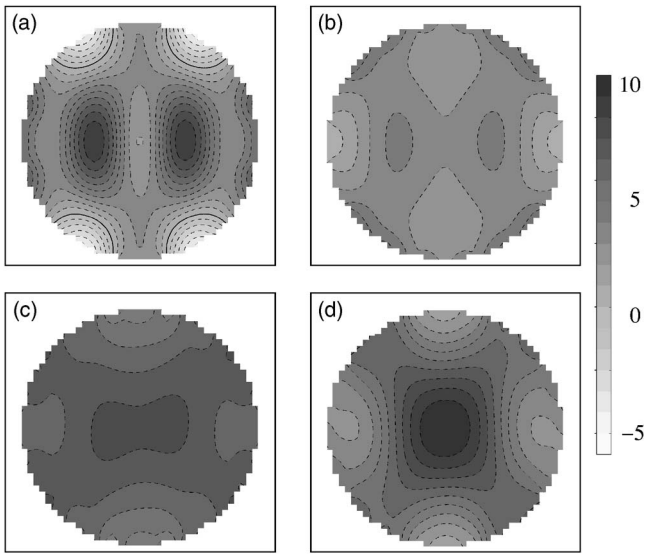

FIG. 3. Profiles of the F modes at $s=50$ nm and $\boldsymbol{R}=0$, calculated for $\boldsymbol{K}=(0,\pi/a)$ (a) and $\boldsymbol{K}=(\pi/a,0)$ (b), corresponding to the highest and lowest frequency of the F band (13.8 and 10.8 GHz, respectively). The profiles calculated for $\boldsymbol{K}=(0,0)$ (c) and $\boldsymbol{K}=(\pi/a,\pi/a)$ (d) (12.0 and 12.4 GHz, respectively) are also shown. A $H=2000$ Oe field is applied along the x axis, i.e., horizontally. The contour plots show the amplitude of the dynamic magnetization (central layer, arbitrary units) with different gray levels; the contour level corresponding to 0 is marked by a solid line. We have plotted the real part of the z component; the profiles of the y component are very similar but purely imaginary. The profiles of the magnetization of other dots in the array ($\boldsymbol{R}\neq 0$) can be obtained using Eq. (1) and remembering that, for the values of $\boldsymbol{K}$ considered here, the exponential assumes either value 1 or −1, depending on $\boldsymbol{R}$.

The profiles of the 1-DE modes are represented in Fig. 5. In this case the oscillations due to the interdot coupling are less pronounced, due to the reduced interaction and the intrinsic nonuniformity of the mode.

We want now to establish a correlation between $\boldsymbol{K}$ and a particular frequency within a band. The frequency-wave-vector dependence can be understood recalling the dispersion curves of the Damon-Eshbach-like modes, that have positive slope, and of the dipolar backwardlike modes, with their negative dispersion.[30] In order to make use of these considerations the first thing to do is to recognize the effective periodicity λ_{eff} of the global dynamic magnetization, taking both the wave vector $\boldsymbol{K}$ and the intrinsic oscillations of the mode in the particle into account. The easiest case is that of the F mode since it has no intrinsic oscillations and the effective wave vector $\boldsymbol{K}_{\mathrm{eff}}=2\pi/\lambda_{\mathrm{eff}}$ coincides with $\boldsymbol{K}$. The collective modes of the array with oscillations perpendicular to the applied field (i.e., in the y direction) show similarity with the DE mode of a film, so that the lowest frequency mode has the smallest effective wave vector, corresponding to $K_y=0$ [see Fig. 6(a), to be compared with Fig. 6(b) which corresponds to the largest effective wave vector along y]. Oscillations parallel to the field (x direction, not shown in Fig. 6 for simplicity) correspond to dipolar BA modes, whose lowest frequency is reached for the maximum

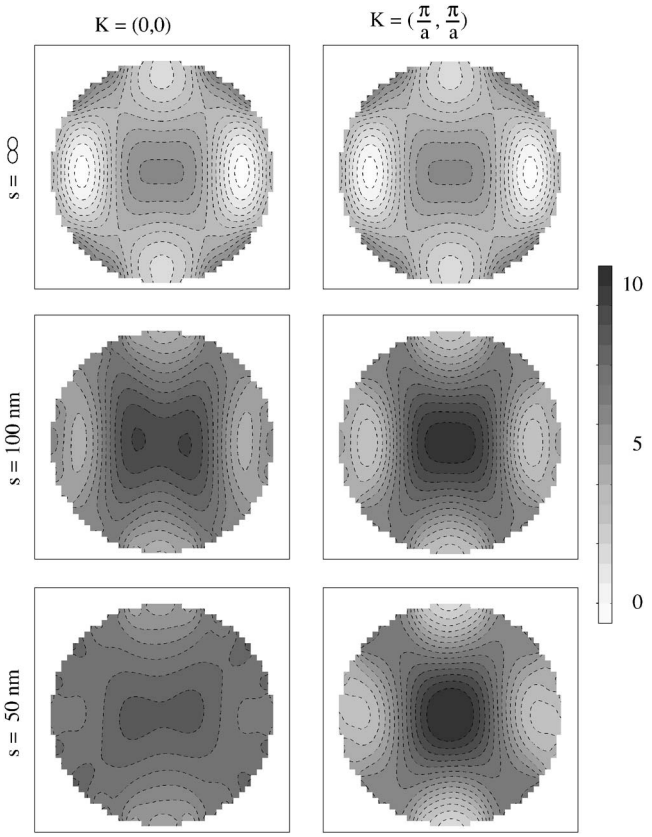

FIG. 4. Evolution of the F mode for $\boldsymbol{K}=(0,0)$ (left column), and $\boldsymbol{K}=(\pi/a,\pi/a)$ (right column) as a function of the interdot separation s.

effective wave vector along x, which corresponds to $K_x=\pi/a$. As a consequence, the curves limiting the F band have $\boldsymbol{K}=(\pi/a,0)$ (lower limit) and $\boldsymbol{K}=(0,\pi/a)$ (upper limit). We note that the dispersion curves published in Ref. 12 for an array of nanosphere (Figs. 5 and 6 therein) are

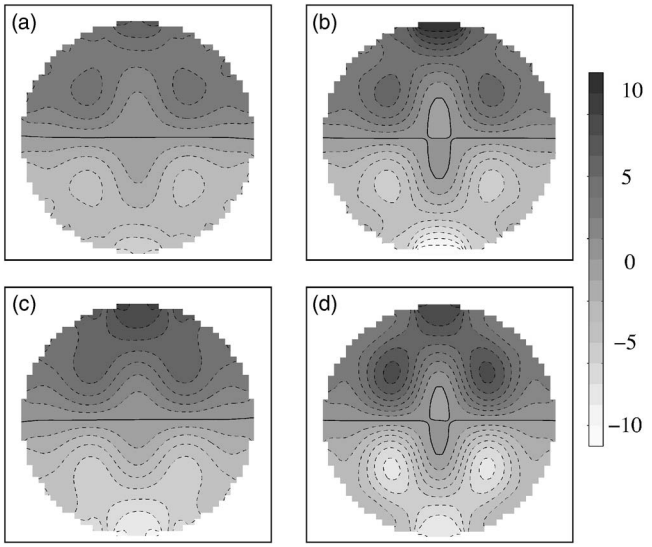

FIG. 5. Profiles of the 1-DE modes at $s=50$ nm and $\boldsymbol{R}=0$, calculated for $\boldsymbol{K}=(0,\pi/a)$ (a), $\boldsymbol{K}=(\pi/a,0)$ (b), $\boldsymbol{K}=(0,0)$ (c), and $\boldsymbol{K}=(\pi/a,\pi/a)$ (d). Other data as for Fig. 3.

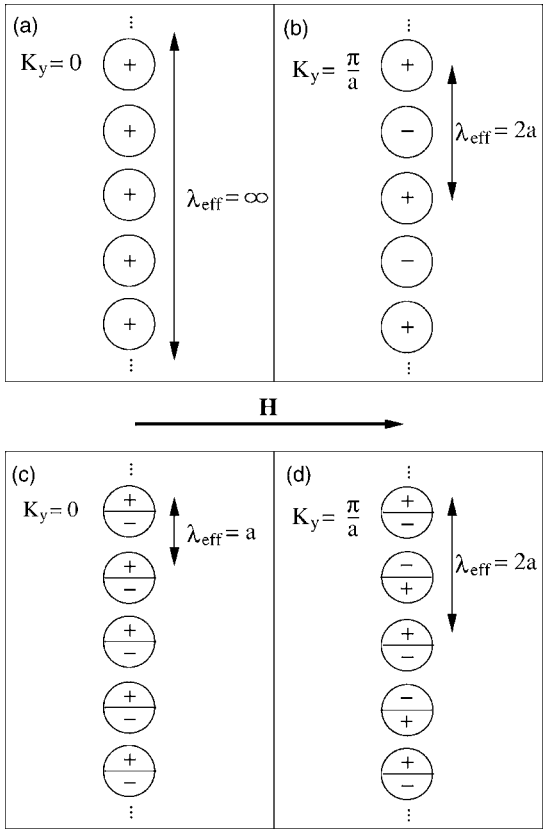

FIG. 6. Sketch of the F (a, b) and 1-DE (c, d) collective modes of a linear array and the corresponding effective periodicity of the entire dynamic magnetization. Two different cases are presented, $K_y=0$ (a, c) and $K_y=\pi/a$ (b, d).

consistent with these considerations, which are independent of the particle shape. When applied to modes other than F, these conclusions must be substantially modified because the effective wave vector no longer coincides with $\boldsymbol{K}$. Let us take the 1-DE mode as an example to illustrate the corresponding argument. In this case, if we consider a linear array of dots placed along the y direction with the 1-DE modes oscillating in-phase ($K_y=0$), the magnetization pattern has a period $\lambda_{\text{eff}}=a$ [Fig. 6(c)]. If, instead, we consider the opposite case ($K_y=\pi/a$), the periodicity is now $\lambda_{\text{eff}}=2a$. The last case, corresponding to the smallest effective wave vector, gives rise to the lowest frequency collective DE-like mode. Along the x direction the discussion made for the F mode still applies. As a result, the lowest curve in the 1-DE band corresponds to $\boldsymbol{K}=(\pi/a,\pi/a)$, and the highest one to $\boldsymbol{K}=(0,0)$. Clearly, the difference between the behavior of the collective F mode and that of the 1-DE mode is due to the oscillation of the magnetization within the particle in the second case, which yields a different λ_{eff} for the same $\boldsymbol{K}$ [compare Figs. 6(a) and 6(c)]. The nature of the boundaries of other bands can be explained along the same line.

The interplay between interdot coupling and cross-section in BLS experiments requires a few comments. The Stokes scattering amplitude is proportional to the following integral:[31–33]

$$\int_{\text{area}} e^{i\boldsymbol{q}\cdot\boldsymbol{r}}\delta\boldsymbol{m}(\boldsymbol{r})d\boldsymbol{r} = \left[\sum_{\boldsymbol{R}\in\text{area}} e^{i(\boldsymbol{q}+\boldsymbol{K})\cdot\boldsymbol{R}}\right]\int_{\text{part}} e^{i\boldsymbol{q}\cdot\boldsymbol{r}}\delta\boldsymbol{m}(\boldsymbol{r})d\boldsymbol{r}, \tag{3}$$

where $\boldsymbol{q}$ is the parallel wave vector exchanged by light and the first integral is extended to the scattering zone (illuminated area). The second term of this equation has been obtained recalling Eq. (1), and the integral is restricted to a single particle; the sum extends to the particles within the illuminated area. In a typical BLS experiment the diameter of the illuminated area can be estimated to be about 20 μm^2,[18] and therefore includes a few hundred of particles, i. e., a number large enough to allow the term in square parentheses of Eq. (3) to approach a Dirac delta. This leads, in principle, to the conservation rule $\boldsymbol{q}=\mp\boldsymbol{K}$ for Stokes or anti-Stokes scattering. It is worth while to note that in the backscattering experiment of Ref. 13, K ranges from 0 to the first Brillouin zone border ($\pi/a=1.257\times10^5$ cm^{-1} maximum, for $s=50$ nm), while $q=4.102\times10^5$ cm^{-1}: this means that the wave-vector conservation rule is never satisfied. This situation is common to many BLS experiments.[34] The visibility of the collective modes in the measured spectra can be explained realizing that the order introduced by the weak interdot dipolar coupling extends over short distances only, being broken by thermal fluctuations on a larger scale. Yet the short-range order plays an important role in determining the frequency of the modes, affected by the dipolar coupling among a few nearest neighbors, as described at the end of Sec. II. In the present application the experiments permit us to estimate the range of the ordering between three and ten particles.

IV. CONCLUSIONS

We have presented a method for studying the dynamic interaction between magnetic particles. This model is suitable for particles of arbitrary shape and periodic arrays of any geometry. The application to a square array of cylindrical particles shows that the calculated frequencies compare well with experimental results, concerning both band formation and frequency changes, as a function of dot separation.

The approach presented in this paper may suggest a method for including the interparticle interactions in micromagnetic standard codes working in time domain. Such programs could be extended by adopting the Bloch conditions of Eq. (1), for calculating both equilibrium states and dynamic fluctuations. In the former case $\boldsymbol{K}=0$ should be used, which is equivalent to the inclusion of periodic boundary conditions, as already implemented in a few codes. In the latter case, the spin modes can be obtained by allowing the wave vector $\boldsymbol{K}$ to span the whole surface Brillouin zone. In this way it would be possible to study the collective modes of large arrays with a restricted number of independent variables.

ACKNOWLEDGMENTS

We thank G. Gubbiotti and co-workers for having pointed out the relevance of a full calculation to compare to their measured data and M. G. Pini for useful discussions. This work was supported by Ministero Università e Ricerca (Grant No. PRIN 2004027288) and by Università di Ferrara (Project No. NANO&NANO).

[1] K. Guslienko, Phys. Lett. A **278**, 293 (2001).
[2] V. Novosad, K. Y. Guslienko, H. Shima, Y. Otani, S. G. Kim, K. Fukamichi, N. Kikuchi, O. Kitakami, and Y. Shimada, Phys. Rev. B **65**, 060402(R) (2002).
[3] K. D. Sorge, A. Kashyap, R. Skomski, L. Yue, L. Gao, R. D. Kirby, S. H. Liou, and D. J. Sellmyer, J. Appl. Phys. **95**, 7414 (2004).
[4] L. J. Heyderman, H. H. Solak, C. David, D. Atkinson, R. P. Cowburn, and F. Nolting, Appl. Phys. Lett. **85**, 4989 (2004).
[5] M. Natali, A. Popa, U. Ebels, Y. Chen, S. Li, and M. E. Welland, J. Appl. Phys. **96**, 4334 (2004).
[6] P. Barpanda, T. Kasama, R. E. Dunin-Borkowski, M. R. Scheinfein, and A. S. Arrott, J. Appl. Phys. **99**, 08G103 (2006).
[7] B. Hillebrands, S. O. Demokritov, C. Mathieu, S. Riedling, O. Büttner, A. Frank, B. Roos, J. Jorzick, A. N. Slavin, B. Bartenhan, C. Chappert, F. Rousseaux, D. Decanini, E. Cambril, A. Cambril, A. Müller, and U. HartmannJ. Magn. Soc. Jpn. **23**, 670 (1999).
[8] J. Jorzick, S. O. Demokritov, B. Hillebrands, B. Bartenlian, C. Chappert, D. Decanini, F. Rousseaux, and E. Cambril, Appl. Phys. Lett. **75**, 3859 (1999).
[9] I. Neudecker, M. Kläui, K. Perzlmaier, D. Backes, L. J. Heyderman, C. A. F. Vaz, J. A. C. Bland, U. Rüdiger, and C. H. Back, Phys. Rev. Lett. **96**, 057207 (2006).
[10] G. N. Kakazei, Y. G. Pogorelov, M. D. Costa, T. Mewes, P. E. Wigen, P. C. Hammel, V. O. Golub, T. Okuno, and V. Novosad, Phys. Rev. B **74**, 060406(R) (2006).
[11] R. Arias and D. L. Mills, Phys. Rev. B **70**, 104425 (2004).
[12] P. Chu, D. L. Mills, and R. Arias, Phys. Rev. B **73**, 094405 (2006).
[13] G. Gubbiotti, M. Madami, S. Tacchi, G. Carlotti, and T. Okuno, J. Appl. Phys. **99**, 08C701 (2006).
[14] J. Shibata and Y. Otani, Phys. Rev. B **70**, 012404 (2004).
[15] A. Y. Galkin, B. A. Ivanov, and C. E. Zaspel, Phys. Rev. B **74**, 144419 (2006).
[16] P. Politi and M. G. Pini, Phys. Rev. B **66**, 214414 (2002).
[17] M. Grimsditch, L. Giovannini, F. Montoncello, F. Nizzoli, G. K. Leaf, and H. G. Kaper, Phys. Rev. B **70**, 054409 (2004).
[18] L. Giovannini, F. Montoncello, F. Nizzoli, G. Gubbiotti, G. Carlotti, T. Okuno, T. Shinjo, and M. Grimsditch, Phys. Rev. B **70**, 172404 (2004).
[19] G. Gubbiotti, G. Carlotti, T. Okuno, M. Grimsditch, L. Giovannini, F. Montoncello, and F. Nizzoli, Phys. Rev. B **72**, 184419 (2005).
[20] V. M. Rozenbaum, V. M. Ogenko, and A. A. Chuiko, Sov. Phys. Usp. **34**, 883 (1991).

[21] E. Rastelli, S. Regina, and A. Tassi, Phys. Rev. B **66**, 054431 (2002).

[22] A. A. Fraerman and M. V. Sapozhnikov, J. Magn. Magn. Mater. **192**, 191 (1999).

[23] P. Politi, M. G. Pini, and R. L. Stamps, Phys. Rev. B **73**, 020405(R) (2006).

[24] R. P. Cowburn, D. K. Koltsov, A. O. Adeyeye, M. E. Welland, and D. M. Tricker, Phys. Rev. Lett. **83**, 1042 (1999).

[25] M. Grimsditch, Y. Jaccard, and I. K. Schuller, Phys. Rev. B **58**, 11539 (1998).

[26] A. J. Newell, W. Williams, and D. J. Dunlop, J. Geophys. Res. **98**, 9551 (1993).

[27] M. E. Schabes and A. Aharoni, IEEE Trans. Magn. **MAG-23**, 3882 (1987).

[28] J. Jorzick, C. Krämer, S. O. Demokritov, B. Hillebrands, E. Sondergard, M. Bailleul, C. Fermon, U. Memmert, A. N. Müller, A. Kounga, U. Hartmann, and E. Tsymbalt, J. Magn. Magn. Mater. **226–230**, 1835 (2001).

[29] M. G. Cottam and A. N. Slavin, in *Linear and Nonlinear Spin Waves in Magnetic Films and Superlattices*, edited by M. G. Cottam (World Scientific, Singapore, 1994), p. 1.

[30] B. A. Kalinikos, in *Linear and Nonlinear Spin Waves in Magnetic Films and Superlattices*, edited by M. G. Cottam (World Scientific, Singapore, 1994), p. 89.

[31] L. D. Landau and E. Lifshitz, *Electrodynamics of Continuous Media* (Pergamon, Oxford, 1960).

[32] J. Jorzick, S. O. Demokritov, C. Mathieu, B. Hillebrands, B. Bartenlian, C. Chappert, F. Rousseaux, and A. N. Slavin, Phys. Rev. B **60**, 15194 (1999).

[33] J. F. Cochran and J. R. Dutcher, J. Magn. Magn. Mater. **73**, 299 (1988).

[34] S. O. Demokritov and B. Hillebrands, in *Spin Dynamics in Confined Magnetic Structures I*, Springer Series in Topics Applied Physics No. 83, edited by B. Hillebrands and K. Ounadjela (Springer, Berlin, 2002), p. 65.